

**WSRT and VLA Observations of the 6 cm and 2 cm lines
of H₂CO in the direction of W 58 C1(ON 3) and W 58 C2**

Hélène R. Dickel^{1,2}

Astronomy Department, University of Illinois,, 1002 W. Green Street, Urbana, IL 61801

lanie@astro.uiuc.edu

W. M. Goss

National Radio Astronomy Observatory P.O. Box O, Socorro, NM 87801

mgoss@nrao.edu

and

C. G. De Pree

*Department of Physics and Astronomy, Agnes Scott College, 141 East College Avenue, Decatur,
GA 30030*

cdepree@herschel.agnesscott.edu

ABSTRACT

Absorption in the $J_{K_-,K_+} = 2_{11} - 2_{12}$ transition of formaldehyde at 2 cm towards the ultracompact HII regions C1 and C2 of W 58 has been observed with the Very Large Array with an angular resolution of $\sim 0.2''$ and a velocity resolution of $\sim 1 \text{ km s}^{-1}$. The high resolution continuum image of C1 (also known as ON 3) shows a partial shell which opens to the NE. Strong H₂CO absorption is observed against W 58 C1. The highest optical depth ($\tau > 2$) occurs in the SW portion of C1 near the edge of the shell, close to the continuum peak. The absorption is weaker towards the nearby, more diffuse compact HII region C2, $\tau \leq 0.3$. The H₂CO velocity (-21.2 km s^{-1}) towards C1 is constant and agrees with the velocity of CO emission, mainline OH masers, and the H76 α recombination line, but differs from the velocity of the 1720 MHz OH maser emission ($\sim -13 \text{ km s}^{-1}$).

Observations of the absorption in the $J_{K_-,K_+} = 1_{10} - 1_{11}$ transition of formaldehyde at 6 cm towards W 58 C1 and C2 carried out earlier with the Westerbork Aperture

¹Visiting Astronomer, ASTRON, P.O. Box 2, 7990AA Dwingeloo, The Netherlands

²Visiting Professor, Astronomical Institute 'Anton Pannekoek', University of Amsterdam, Kruislaan 403, 1098SJ, Amsterdam, The Netherlands

Synthesis Telescope at lower resolution ($\sim 4'' \times 7''$) show comparable optical depths and velocities to those observed at 2 cm. Based on the mean optical depth profiles at 6 cm and 2 cm, the volume density of molecular hydrogen $n(\text{H}_2)$ and the formaldehyde column density $N(\text{H}_2\text{CO})$ were determined. The $n(\text{H}_2)$ is $\sim 6 \times 10^4 \text{ cm}^{-3}$ towards C1. $N(\text{H}_2\text{CO})$ for C1 is $\sim 8 \times 10^{14} \text{ cm}^{-2}$ while that towards C2 is $\sim 8 \times 10^{13} \text{ cm}^{-2}$.

Subject headings: interstellar medium:clouds: W 58 C, ON 3, K3-50 - radio lines:molecular: H_2CO

1. Introduction

The star-forming complex W 58 (Westerhout 1958) at $\ell \sim 70.3$ and $b \sim +1.6$ is located on the far side of the Cygnus spiral arm at a distance of 8.7 Kpc (Israel 1976). The region has been imaged in the continuum by Wynn-Williams (1969) and Israel (1976), in CO by Israel (1981), and in HI by Read (1981). The complex includes the optical nebulae NGC 6857 and K3-50 (Perek and Kohoutek 1967). At radio wavelengths, Wynn-Williams (1969) detected three main components A, B, and C. Component A coincides with optical nebula K3-50. At high resolution ($< 4''$), component C is resolved into ultracompact HII regions (UCHII regions) W 58 C1 and W 58 C2 (Harris 1975). Additional faint extensions to the emission from C1 are designated C3 (to NW) and C4 (to SE) by Colley and Scott (1977). Elldér et al. (1969) and Rubin and Turner (1969) independently discovered a 1720 MHz OH maser which was later designated ON 3 (Winnberg 1970). Wynn-Williams et al. (1974) determined an accurate position for ON 3 which can be associated with the UCHII region C1.

Righini-Cohen et al. (1979) observed the hydrogen Brackett α line at $4 \mu\text{m}$ towards W 58 and derived a visual extinction of ~ 100 magnitudes towards C1 and ~ 25 magnitudes towards C2. Van Gorkom et al. (1981) observed W 58 in the H109 α recombination line at 6 cm with the Westerbork Radio Synthesis Telescope (WSRT) with an angular resolution of $\sim 10''$. The H109 α line towards C1 has an LSR velocity of $-16 \pm 3 \text{ km s}^{-1}$, compared to a typical velocity of -22 km s^{-1} for the neutral gas [e.g. CO, Israel (1981)]. From this observed velocity difference and the high extinction seen towards component C1, both Israel (1981) and van Gorkom et al. (1981) favored the “blister” model for the overall molecular cloud with UCHII regions C1 and C2 located on the far side of the cloud. Howard et al. (1996) reached the same conclusion from near-infrared observations of the continuum emission and Brackett α and γ lines.

Observations with the Very Large Array (VLA) at 2 cm with $\sim 2''$ resolution by De Pree et al. (1994) reveal a core-halo structure in the continuum for C1 and with a velocity of the H76 α line of $-22 \pm 2 \text{ km s}^{-1}$, in agreement with the velocity of the molecular gas. VLA observations at an even higher resolution of $\sim 0.1''$ by Turner and Matthews (1984) show a shell-type structure in the continuum similar to that of W 3(OH), but with a break in the shell to the east.

Forster et al. (1981) observed W 58 C in the $J_{K_-,K_+} = 1_{10} - 1_{11}$ transition of formaldehyde at 6 cm with the WSRT with a resolution of $\sim 10''$. They found strong H₂CO absorption towards C1 with an optical depth τ of ~ 2 and weaker absorption with $\tau \sim 0.25$ towards C2. W 58 C1 (ON3) exhibits the deepest H₂CO absorption of any of the UCHII regions observed by Forster et al. (1981) at 6 cm with $\sim 5''$ resolution (Forster et al. 1982; Forster and Boland 1982). In this paper, we present observations of the $J_{K_-,K_+} = 2_{11} - 2_{12}$ transition of H₂CO at 2 cm towards both C1 and C2 made with the VLA with a resolution of $\sim 0.2''$. These observations were obtained in order to determine whether the molecular gas towards C1 has the same toroidal structure as had been determined for the shell source W 3(OH) by Dickel and Goss (1987). The new 2 cm observations are described in § 2 and the data are presented in § 3. In § 4 mean H₂CO column densities and H₂ volume densities in the molecular gas towards the UCHII regions are derived from a comparison of the 2 cm and 6 cm H₂CO profiles, using the same procedure as in previous papers of this series [e.g. Dickel and Goss (1987); Dickel et al. (1996)]. The nature of W 58 C1 is discussed in § 5 and the conclusions are summarized in § 6.

2. Observations and Data Processing

Observations of the ortho-formaldehyde absorption towards the UCHII regions C1 and C2 of W 58 were made in the $J_{K_-,K_+} = 1_{10} - 1_{11}$ (hereafter 6 cm H₂CO) and $J_{K_-,K_+} = 2_{11} - 2_{12}$ (hereafter 2 cm H₂CO) transitions. The 6 cm transition was observed with WSRT in 1980 by Forster et al. (1982) with a resolution of $7.2'' \times 3.8''$ (PA=0°). The calibration and processing of the WSRT data are discussed by Forster and Boland (1982).

The 2 cm VLA data were calibrated in the spatial frequency (u, v) domain in the standard manner and then imaged using the “Pipeline” system (Brouw 1981). Uniform weighting was used during the Fourier transformation resulting in a synthesized beam of $0.11'' \times 0.10''$ (PA=−88.5°). In addition, the u, v data were self-calibrated using the continuum image and then Fourier transformed with natural weighting resulting in a synthesized beam of $0.25'' \times 0.22''$ (PA=−84.0°). The instrumental parameters are listed in Table 1 for both the 6 cm and 2 cm data sets. The 2 cm data were processed and analyzed using the Astronomical Image Processing System (AIPS) software of NRAO. No primary beam correction was applied because the field of view is centered on C1 and the intensity of C2 is diminished by a factor of only a few percent. The coordinates for the field center are given in Table 1 for both J2000.0 and B1950.0 (as originally specified for the observations). A simple, yet accurate, conversion from B1950.0 to J2000.0 was applied to the small regions around C1 and C2. Only the larger image of the entire region (Fig. 1a) remains with B1950.0 coordinates; this provides an easy comparison with earlier images.

Two “CLEANED” continuum images were made at 2 cm: one with uniform weighting to obtain the highest resolution and the self-calibrated image with natural weighting to obtain the best sensitivity to the more extended emission. Channel images of the absorbed continuum due to the H₂CO molecule were made for the 2 cm line.

Images of the H₂CO optical depths (τ) were obtained from the continuum image (T_c) and from the channel images of the absorbed continuum at various velocities (T_ℓ): $\tau = -\ln(T_\ell/T_c)$. Optical depths were calculated only where the signal-to-noise ($S/N = \tau/\sigma_\tau$) was > 2 . Because of the weakness of the continuum, the sensitivity of the line data at the original resolution of $\sim 0.1''$ was inadequate. Therefore, optical depth images with a resolution of $0.24''$ were made.

The 2 cm VLA data are available on the Web at <http://adil.ncsa.uiuc.edu/document/00.HD.01>

3. Data

3.1. Continuum Emission

Continuum images at 2 cm of W 58 C1 (to the west) and C2 (to the east) made with natural weighting are shown in Fig. 1a. The rms σ is $0.5 \text{ mJy beam}^{-1}$ (beam = $0.25'' \times 0.22''$). Fig. 1a shows low-level extended emission surrounding the compact core of C1 which corresponds to the C3 (in NW) and C4 (in SE) components of Colley and Scott (1977). Within the 3σ level, the integrated flux density is $400 \pm 30 \text{ mJy}$ for C1 and $190 \pm 40 \text{ mJy}$ for C2. These flux densities are somewhat lower than the values of $500 \pm 10 \text{ mJy}$ for C1 and $200 \pm 40 \text{ mJy}$ found by De Pree et al. (1994) at the lower resolution of $1.4'' \times 1.1''$. The VLA in A array at 2 cm is insensitive to structures larger than about $4''$. If the missing flux density of $\sim 100 \text{ mJy}$ for C1 were spread over a $4''$ region, then the additional intensity would be equivalent to $\sim 0.7\sigma$ and thus not detected.

A new small source, designated C5 in Fig. 1a, is located to the south of C1 and C2 at (B1950) $\alpha = 19^h 59^m 58.74^s \pm 0.01^s$ and $\delta = 33^\circ 25' 36.2'' \pm 0.1''$ [(J2000) $\alpha = 20^h 01^m 54.34^s$ and $\delta = 33^\circ 34' 00.8''$]. This source has a peak flux density of $3.5 \pm 0.5 \text{ mJ beam}^{-1}$ and an integrated flux density of $18 \pm 2.8 \text{ mJy}$. It's size is $\sim 0.7 \pm 0.1'' \times 0.4 \pm 0.05''$ (PA $\sim 110^\circ \pm 9^\circ$). Balser et al. (2000) measured a flux density of 20 mJy at 3.6 cm for this source which gives a spectral index $\alpha \sim -0.1$.

A continuum image of UCHII region C2 is shown as both grey-scale and with contours in Fig. 1b with a resolution of $0.22''$. C2 appears as a ridge of emission elongated almost north-south with more diffuse emission to the west.

The highest resolution image ($0.11''$) of UCHII region C1 in Fig. 1c clearly shows the partial shell structure with the break to the east. With a sensitivity of 1 mJy beam^{-1} the extended emission is not detected. Contours of the extended emission in the natural weighted image (beam = $0.25'' \times 0.22''$) are shown in Fig. 1d, superposed on a grey-scale presentation of the uniform-weighted, higher-resolution image.

3.2. Formaldehyde Absorption at 2 cm

3.2.1. Spatial Distribution

The 2 cm H₂CO optical depths towards the UCHII region W 58 C1 with a resolution of 0.24'' are presented for nine velocities in Fig. 2 as grey scale images with contours superposed. The S/N ranges from about two at the edges to six - seven just east of the continuum peak. The highest optical depths with $\tau(H_2CO) \geq 2$ occur at a velocity $V_{LSR} = -21.2$ km s⁻¹ along a north-south ridge running across and slightly west of the continuum peak.

The correspondence between H₂CO optical depth and continuum emission is illustrated in Fig. 3 where the 0.11'' resolution continuum contours for C1 from Fig. 1c are superposed on the grey scale image of the optical depth for $V_{LSR} = -21.2$ km s⁻¹. The close spatial correspondence between the high formaldehyde opacity and the C1 continuum peak indicates that this molecular gas is probably physically associated with the UCHII region.

3.2.2. Velocity Structure

The width of the H₂CO line at 2 cm $\Delta V(FWHM)$ is between 2 and 3 km s⁻¹ towards C1. The velocity of the line is essentially constant across the UCHII region with $V_{LSR} \sim -21.2$ km s⁻¹; there is a variation of, at most, ~ 0.3 km s⁻¹. At the position where the optical depth is highest, along a ridge just to the west of the continuum maximum, the H₂CO velocity is slightly more positive than the average ($\langle V_{LSR} \rangle = -21.1$ km s⁻¹). To the east of the continuum maximum where there is a hole and break in the HII shell, the H₂CO velocity is more negative ($\langle V_{LSR} \rangle = -21.4$ km s⁻¹); here the molecular gas is expanding away from the UCHII region.

3.3. Spatially integrated H₂CO Profiles at 6 cm and 2 cm

Spatially-integrated H₂CO absorption profiles at 6 cm towards the continuum peaks of W 58 C1 and C2 shown in Fig. 4 were taken from Forster et al. (1982). In order to compare the 6 cm and 2 cm data, the 2 cm H₂CO line data were also integrated over each source - over the area encompassed by the outer contour of Fig. 1d for C1 and by the outer contour of Fig. 1b for C2. These spatially integrated profiles are shown in Fig. 5.

4. Mean H₂ Densities and H₂CO Column Densities

4.1. Determination of $n(H_2)$ and $N(H_2CO)$

The method described by Dickel et al. (1986) and Dickel and Goss (1987) was used to obtain the H₂ spatial density $n(H_2)$, and the H₂CO column density $N(H_2CO)$. The procedure is based on radiative transfer calculations using the Sobolev approximation. In the H₂ density range $10^3 \leq n(H_2) \leq 10^6$, the strength of the H₂CO absorption at 2 cm relative to that at 6 cm is related to the H₂ density while the strength of the absorption at 6 cm is sensitive to variations in H₂CO column density.

Input parameters for the radiative transfer calculations of Dickel et al. (1986) are the kinetic temperature T_K , the molecular hydrogen density $n(H_2)$, the radius of the cloud R , maximum velocity V , and the number density of ortho H₂CO molecules in all levels n_t . After the populations of the levels x_j were determined for particular values of T_K and $n(H_2)$ and a range of n_t , the expected optical depths τ_{jk} for the 6 cm and 2 cm lines were calculated according to the following relationship:

$$\tau_{jk} = \left[\frac{c^3}{8\pi} \frac{A_{jk} g_j}{\nu_{jk}^3} \right] \cdot [x_k - x_j] \cdot \left[\frac{n_t}{(dv/dr)} \right] \quad (1)$$

or

$$\tau_{jk} \propto [x_k - x_j] \cdot n(H_2) \cdot A(\text{ortho } H_2CO), \quad (2)$$

where the relative abundance per velocity gradient $A(\text{ortho } H_2CO)$ is given by

$$A(\text{ortho } H_2CO) = \frac{[\text{ortho } H_2CO]}{[H_2]} \cdot \frac{1}{(V/R)} = \frac{n_t}{n(H_2)} \cdot \frac{1}{(dv/dr)}. \quad (3)$$

Dickel and Goss (1987) present curves of constant $n(H_2)$ and constant $A(\text{ortho } H_2CO)$ as functions of $r = \frac{\tau(6cm)}{\tau(2cm)}$ and $\tau(6cm)$ for $T_K = 40$ K and $T_K = 60$ K.

With $[H_2CO]/[\text{ortho } H_2CO] = 1.33$ and A in units of $(\text{km s}^{-1} \text{ pc}^{-1})^{-1}$, $N_V(H_2CO)$ in units of $\text{cm}^{-2} (\text{km s}^{-1})^{-1}$ is defined as

$$N_V(H_2CO) = 4.1 \cdot 10^{18} \cdot A(\text{ortho } H_2CO) \cdot n(H_2). \quad (4)$$

Multiplying $N_V(H_2CO)$ by the FWHM line width ΔV , yields the H₂CO column density, $N(H_2CO)$.

There is no measurement of the kinetic temperature towards C1 but a radiation temperature of 26 K (with $T_K \sim 30$ K) has been observed by Phillips and Mampaso (1991) in the CO J=3 – 2 transition with 30'' resolution toward K3-50 ($\sim 2'$ to SW of C1). Other molecular clouds with embedded HII regions such as DR 21, W 49 A north, and W 51 A have kinetic temperatures between 40 K and 50 K (Phillips et al. 1988). Fortunately, the radiative transfer calculations are insensitive to kinetic temperature. For example, changing T_K by 20 K changes $n(H_2)$ and $N(H_2CO)$ by less than 15% whereas observational uncertainties of 10% in τ_{jk} can produce uncertainties on the order of 50% in these quantities. Therefore, the radiative transfer results for $T_K = 40$ K from Dickel and Goss (1987) were used to determine $n(H_2)$ and $N_V(H_2CO)$ for C1.

4.2. Results for W 58 C1 and C2

It is not possible to determine values of $n(H_2)$ and $N_V(H_2CO)$ for different regions of the sources because of the limited resolution of the 6 cm observations. Therefore, mean values were derived for W 58 C1 and C2 from the spatially integrated profiles shown in Figs. 4 and 5. The resulting $n(H_2)$ and $N_V(H_2CO)$ for C1 are shown in Fig. 6. Although the sensitivity is insufficient to obtain a good determination of $n(H_2)$ for C2, an estimate of $N_V(H_2CO)$ can be determined from the 6 cm optical depth because of its dependence on H_2CO column density.

The mean H_2 density for the molecular gas in front of C1 is in the range $(4-8)\times 10^4 \text{ cm}^{-3}$ and the H_2CO column density is $N(H_2CO) = (8\pm 4) \times 10^{14} \text{ cm}^{-2}$. The corresponding value of the column density of the molecular gas in front of C2 is $\sim 10^{14} \text{ cm}^{-2}$.

Using the Jenkins and Savage (1974) relationship between visual extinction A_V and $N(H_2)$, values of $N(H_2)$ were derived from the A_V given by Righini-Cohen et al. (1979) ($A_V \sim 25$ magnitudes in front of C2 and ~ 100 magnitudes in front of C1). The derived relative abundance $[H_2CO]/[H_2]$ of about 2×10^{-9} in the direction of C2 is similar to the $(1-2)\times 10^{-9}$ determined for W 3A, W 49A north and south, and DR 21A whereas the higher relative abundance of $\sim 6\times 10^{-9}$ towards C1 is closer to the $\sim 5\times 10^{-9}$ found for the torus around W 3(OH) and towards DR 21C [see Dickel and Goss (1990)].

5. The Nature of W 58 C1

Following Wood and Churchwell (1989)'s classification scheme for UCHII regions, W 58 C1 is either a cometary UCHII region like W 49 S (Gaume and Mutel 1987) or a broken shell UCHII region such as W 3(OH) (Dickel and Goss 1987). These two scenarios are explored in the next two sections (§§ 5.1. and 5.2.).

5.1. Cometary UCHII Region - Comparison with Bow-Shock Models

According to models explaining cometary UCHII regions as stellar-wind bow shocks, the ionizing star of C1 is expected to be moving towards the southwest and observations at higher resolution should show a steep gradient in the continuum emission on the southwest side [van Buren et al. (1990); van Buren and Mac Low (1992)]. In addition, there should be a relative velocity of approach between the molecular and ionized gas of several km s^{-1} depending on the velocity of the ionizing star. From spatially integrated $H76\alpha$ radio recombination line profiles, De Pree et al. (1994) find a mean velocity of the ionized gas of $V_{LSR} = -22 \pm 2 \text{ km s}^{-1}$, comparable to that of the molecular gas - indicating no relative motions between them.

The OH masers are expected to be located in the shocked shell (not in the pre-shock material).

In this case, the measured velocity of the 1720 MHz OH masers [$V_{LSR} \sim -13 \text{ km s}^{-1}$ (Winnberg 1970)] would indicate that the star is moving not only to the west but also away from the observer. Because the accuracy of the 1720 MHz OH position is insufficient to precisely locate the masers relative to the continuum source, no firm conclusions can be made at this time regarding the applicability of the stellar-wind, bow shock model to C1.

5.2. Broken Shell - Comparison with W 3(OH)

With the current data, the most favorable model for C1 is that of a broken shell, similar to the shell source W 3(OH). Both the 6 cm and the 2 cm H_2CO absorption lines towards W 3(OH) were imaged using the VLA by Dickel and Goss (1987). As in the case of W 58 C1, pronounced changes in optical depth across W 3(OH) are also observed.

For W 3(OH) - at the velocities of the OH masers, the 2 cm H_2CO absorption only covers the western half of the W 3(OH) in contrast to the more ubiquitous 6 cm H_2CO absorption. The data are consistent with a toroidal model for the dense molecular gas surrounding W 3(OH). The shell appearance of the HII region is due to the ionization of the molecular torus. The H_2 density is much higher in the torus than in the surrounding envelope of molecular gas. An accurate determination of the H_2 density in the torus is not possible from the mean optical depths alone; this requires detailed imaging in two transitions [as was done by Dickel and Goss (1987) for W 3(OH).]

For W 58 C1 - the optical depth of the 2 cm H_2CO absorption varies across this source with the highest values associated with a ridge at the southwest edge of the bright continuum arc. Observations towards the region of the SE break in the continuum shell indicate that the molecular gas may be expanding away from the UCHII region towards the observer. The derived mean H_2 density of the absorbing gas towards C1 is similar to that found in the overall molecular cloud surrounding W 3(OH), while the mean relative H_2CO abundance towards C1 is similar to that derived for the W 3(OH) molecular torus.

A significant increase in the H_2 density where the 2 cm transition has its maximum optical depth would be further evidence that a molecular torus also surrounds C1. High sensitivity and resolution spatial imaging in the 1 cm transition of H_2CO in combination with the existing 2 cm data is required for a determination of the H_2 density across C1.

The observations of the continuum emission and $\text{H}92\alpha$ observations at 3.6 cm of Balser et al. (2000) not only support the broken shell model for W 58 C1 but show evidence for a bipolar outflow. Our observations of the continuum at 2 cm with $\sim 0.2''$ resolution (Fig. 1a) reveal an elongated envelope in the NW to SE direction, corresponding to components C3 and C4 of Colley and Scott (1977). The 3.6 cm data with $2''$ resolution show that the ionized gas extends to more than twice the distance shown in Fig. 1a. There is a velocity gradient in the $\text{H}92\alpha$ recombination lines from $V_{LSR} \sim -18 \text{ km s}^{-1}$ in the NW to $\sim -24 \text{ km s}^{-1}$ in the SE indicating that this is a bipolar outflow and that the systemic velocity of C1 is the same as that of the molecular cloud

($V_{LSR} \sim -21 \text{ km s}^{-1}$). Some H_2CO molecules are apparently entrained in the ionized outflow, albeit at a reduced velocity; this expanding gas arises from the gap in the UCHII shell.

6. Conclusions

H_2CO absorption has been observed at 2 cm with the VLA towards the UCHII regions C1 and C2 of the W 58 star-forming region. Weak absorption with $\tau \leq 0.3$ is seen towards C2. A prominent line with $\tau > 2$ is observed in the SW part of C1 close to the continuum peak and is physically associated with this UCHII region. The H_2CO line at 2 cm is narrow with $\Delta V \sim 2 \text{ km s}^{-1}$ and V_{LSR} of $\sim -21.2 \text{ km s}^{-1}$. This velocity is in good agreement with the $\text{H}76\alpha$ recombination line velocity ($-22 \pm 2 \text{ km s}^{-1}$). The molecular gas in the east towards the gap in the UCHII shell is expanding by $\sim 0.3 \text{ km s}^{-1}$ relative to the molecular gas with large integrated opacity near the western edge of the shell.

A value of $n(\text{H}_2) \sim 6 \times 10^4 \text{ cm}^{-3}$ and of $N(\text{H}_2\text{CO}) \sim 8 \times 10^{14} \text{ cm}^{-2}$ is determined for the absorbing molecular gas in front of the UCHII region C1 from a comparison of the mean H_2CO profiles at 6 cm and at 2 cm. The $N(\text{H}_2\text{CO})$ towards C2 is estimated to be 0.1 that found towards C1. The relative abundance $[\text{H}_2\text{CO}]/[\text{H}_2]$ is $\sim 6 \times 10^{-9}$ towards C1 and $\sim 2 \times 10^{-9}$ towards C2.

W 58 C1 exhibits a core-halo structure with the core appearing as a "broken shell". The 2 cm absorption is strongest at the edge of the bright arc of continuum emission and suggests that the molecular gas might also be in a dense toroid around the UCHII similar to W3(OH). To confirm this will require sensitive, high resolution imaging of the 1 cm transition of H_2CO . To completely rule out the possibility of a "cometary" (bow-shock) model for W 58 C1, higher resolution imaging of radio recombination lines, the 1720 OH maser emission, and the continuum emission are required.

Partial support of the initial stages of this research from NATO grant 138.80 to HRD and WMG is gratefully acknowledged. HRD acknowledges partial support from the Laboratory of Astronomical Imaging which is operated with funds provided by the Berkeley- Illinois-Maryland Association; such research was partially supported by the National Science Foundation through grant 96-13999 to the University of Illinois. The National Radio Astronomy Observatory is a facility of the National Science Foundation operated under cooperative agreement by Associated Universities, Inc.. The Westerbork Synthesis Radio Telescope is operated by the ASTRON (Netherlands Foundation for Research in Astronomy) with support from the Netherlands Foundation for Scientific Research NWO. HRD wishes to thank the Astronomical Institute of the University of Amsterdam and the ASTRON for their hospitality during the final stages of this project. CGD thanks NRAO for hospitality in Socorro, NM where some of this work was carried out.

REFERENCES

- Balser, D. S., Goss, W. M., and De Pree, C. G., 2000, *AJ*, in press
- Brouw, W. N. 1981, “Gridder System” (Pipeline), *VLA Computer Memoranda* 159, 160
- Colley, D., and Scott, P. F. 1977, *MNRAS*, 181, 703
- De Pree, C. P., Goss, W. M., Palmer, P., and Rubin, R. H. 1994, *ApJ*, 428, 670
- Elldér, J., Rönnäng, B., and Winnberg, A. 1969, *Nature*, 222, 67
- Dickel, H. R., and Goss, W. M. 1987, *A&A*, 185, 271
- Dickel, H. R., and Goss, W. M. 1990, *ApJ*, 351, 189
- Dickel, H. R., Goss, W. M., and Condon, G. R. 1996, *ApJ*, 460, 716
- Dickel, H. R., Goss, W. M., Rots, A. H., and Blount, H. M. 1986, *A&A*, 162, 221
- Forster, J. R., Goss, W. M., Dickel, H. R., and Habing, H. J. 1981, *MNRAS*, 197, 513
- Forster, J. R., and Boland, W. 1982, *A&A*, 114, 109
- Forster, J. R., Goss, W. M., and Dickel, H. R. 1982, *Regions of Recent Star Formation*, R. S. Roger and P.E. Dewdney, *Ap&SS*, 93, 409
- Gaume, R. A., and Mutel, R. L. 1987, *ApJS*, 65, 193
- Harris, S. 1975, *MNRAS*, 170, 139
- Howard, E. M., Pipher, J. L., Forrest, W. J., De Pree, C. G. 1996, *ApJ*, 460, 744
- Israel, F. P. 1976, *A&A*, 48, 193
- Israel, F. P. 1980, *ApJ*, 236, 465
- Jenkins, E. B., and Savage, B. D. 1974, *ApJ*, 187, 243
- Perek, L., and Kohoutek, L. 1967, *Catalog of Galactic Planetary Nebulae*, Acad. Publ. House, Prague
- Phillips, J. P., and Mampaso, A. 1991, *A&AS*, 88, 189
- Phillips, J. P., White, G. J., Rainey, R., Avery, L. W., Richardson, K. J., Griffin, M. J., Cronin, N. J., Monteiro, T., and Hilton, J. 1988, *A&A*, 190, 289
- Read, P. L. 1981, *MNRAS*, 195, 371
- Righini-Cohen, G., Simon, M., and Young, E. T. 1979, *ApJ*, 232, 782

- Rubin, R. H., and Turner, B. E. 1969, *ApJ*, 157, L41
- Turner, B. E., and Matthews, H. E. 1984, *ApJ*, 277, 164
- van Buren, D., and Mac Low, M.-M. 1992, *ApJ*, 394, 534
- van Buren, D., Mac Low, M.-M., Wood, D. O. S., and Churchwell, E. 1990, *ApJ*, 353, 570
- van Gorkom, J. H., Shaver, P. A., Pottasch, S. R., Blair, G. N., and Matthews, H. E. 1981, *A&A*, 94, 259
- Westerhout, G. 1958, *Bull. Astron. Inst. Netherlands*, 14, 215
- Winnberg, A. 1970, *A&A*, 9, 259
- Wood, D. O. S., and Churchwell, E. 1989, *ApJS*, 69, 831
- Wynn-Williams, C. G. 1969, *Astrophys. Lett.*, 3, 195
- Wynn-Williams, C. G., Werner, M. W., and Wilson, W. J. 1974, *ApJ*, 187, 41

Fig. 1.— Continuum images of the W 58 C region made with the VLA at a wavelength of 2 cm. Positive contours are solid lines and negative ones are dashed. The first figure (1a) is with B1950.0 coordinates; all subsequent figures are with J2000.0 coordinates.

a) Natural-weight, self-calibrated continuum image of W 58 C at a resolution of $0.25'' \times 0.22''$ (PA= -84.0°). UCHII region C1 and C2 are to the west and east, respectively. Contour levels are -4, -2, 2 ($\sim 4\sigma$), 4, 8, 16, 32, and 64 mJy beam $^{-1}$. The (natural-weighted) beam is shown in the lower left corner.

b) Grey-scale image plus contours of the emission from UCHII region W 58 C2 with a resolution of $0.22''$. Contours are -2.5, 2.5 ($\sim 3\sigma$), 4, 5.5, and 7 mJy beam $^{-1}$. The (uniform-weighted) beam is shown at the lower left.

c) Continuum image of UCHII region W 58 C1 (ON 3) with a resolution of $0.11''$. Contours are -2.5, 2.5 ($\sim 3\sigma$), 5, 7.5, 10, 12.5, and 13.6 mJy beam $^{-1}$. The (uniform-weighted) beam is shown at the lower left.

d) Overlay of three outer contours of the lower resolution ($0.25'' \times 0.22''$) continuum image on the higher resolution ($0.11''$), grey scale image of the UCHII region W 58 C1. The contours are 5, 10, and 20 mJy beam $^{-1}$. The first contour is at the $\sim 10\sigma$ level and encompasses the area over which the mean profile shown in Fig. 5 was obtained.

Fig. 2.— Selected channel images of the H₂CO optical depth in the $2_{11} - 2_{12}$ transition at 2 cm towards UCHII region W 58 C1 shown in grey scale with contours superposed. The $0.24''$ beam is shown in the first panel. The LSR velocity for the channel is given at the top of each panel. For the fourth panel with $V(LSR) = -21.2$ km s $^{-1}$, the contours are $\tau = 1.0$ to 2.5 by 0.5 , and 2.9 . For panels 2, 3, and 5, the contours are $\tau = 0.5$ and 1.0 . For the remainder, the contour is $\tau = 0.25$.

Fig. 3.— Grey scale image of the 2 cm H₂CO optical depth at $V(LSR) = -21.2$ km s $^{-1}$ towards W 58 C1 at a resolution of $0.24''$ with continuum contours from Fig. 1c superposed. The optical depth scale is given at the top.

Fig. 4.— Spatially integrated profiles of the 6 cm H₂CO absorption towards W 58 C observed with the WSRT: towards component C1 at the bottom and towards C2 at the top. The left-hand side gives the flux density scale in mJy and the right-hand side gives the H₂CO optical depth scale. The ($\pm 1 \sigma$) rms error bars are shown; $\sigma = 11.3$ mJy for both C1 and C2.

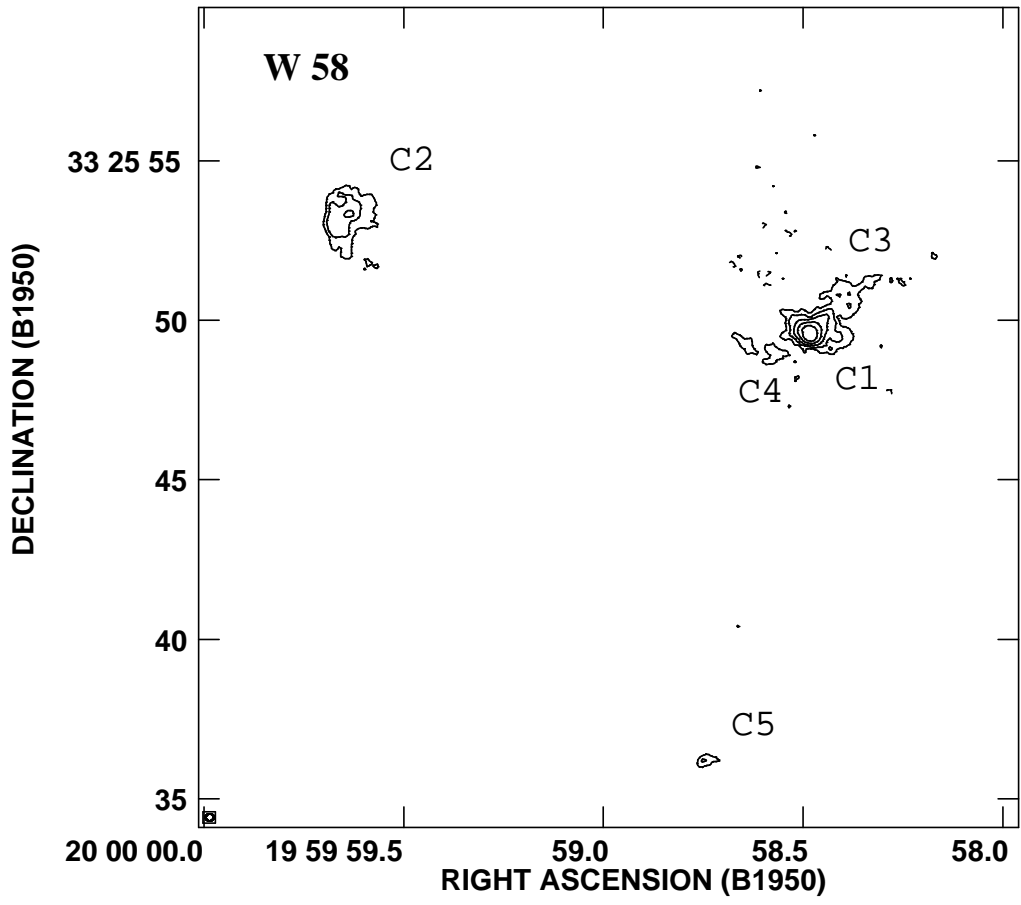
Fig. 5.— Spatially integrated profiles of the 2 cm H₂CO absorption towards W 58 C observed with the VLA: towards component C1 at the bottom and towards C2 at the top. The left-hand side gives the flux density scale in mJy and the right-hand side gives the H₂CO optical depth scale. The ($\pm 1 \sigma$) rms error bars are shown; $\sigma = 8.4$ mJy for C1 and $\sigma = 11.5$ mJy for C2.

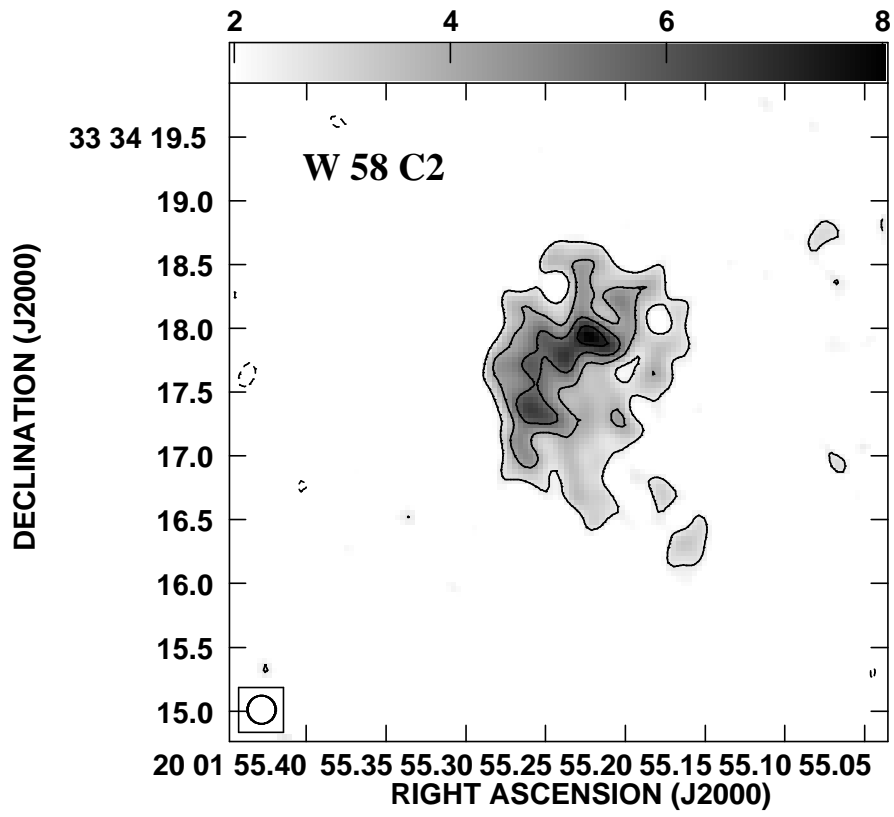
Fig. 6.— Profiles of mean H₂ volume density, $n(H_2)$, shown at the bottom and mean H₂CO column density per velocity interval, $N_V(H_2CO)$, shown at the top as a function of velocity towards W 58 C1. The error bars are $\pm 1 \sigma$. The dashed horizontal line in the upper panel indicates an

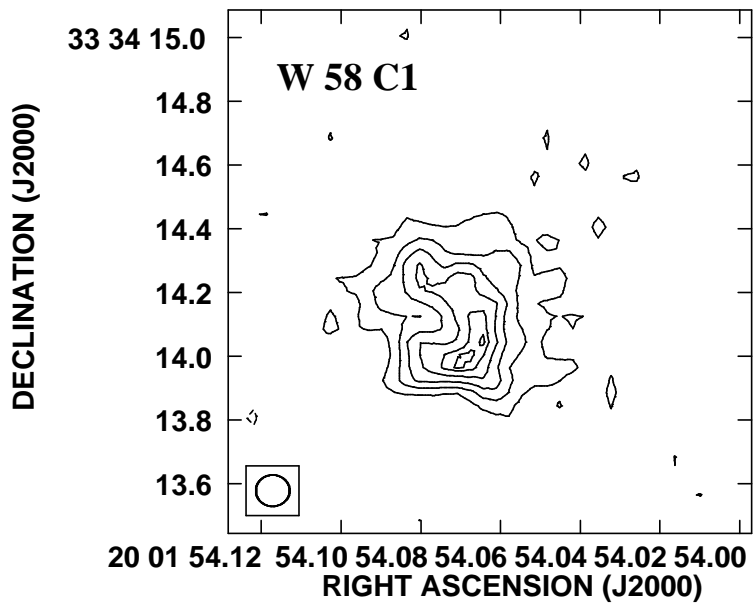
approximate value for $N_V(H_2CO)$ for C2.

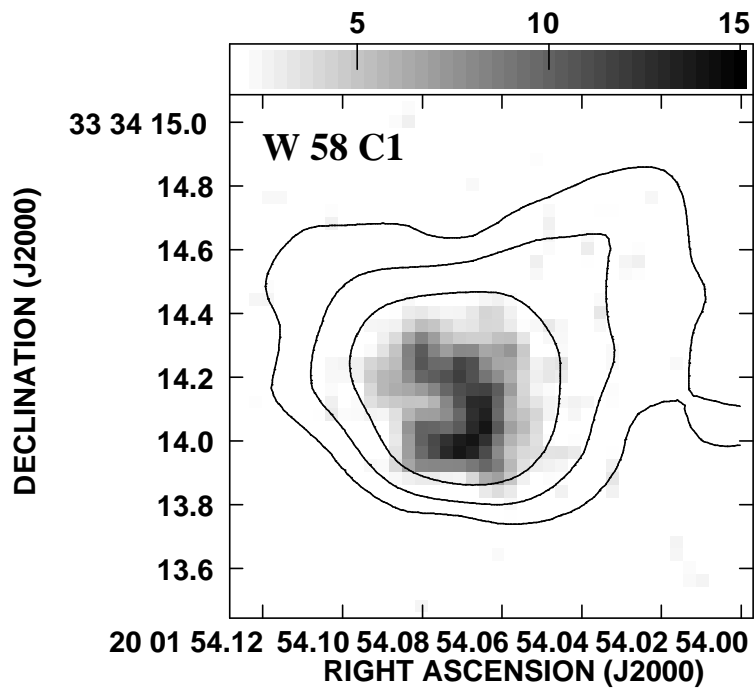
Table 1. Instrumental Parameters

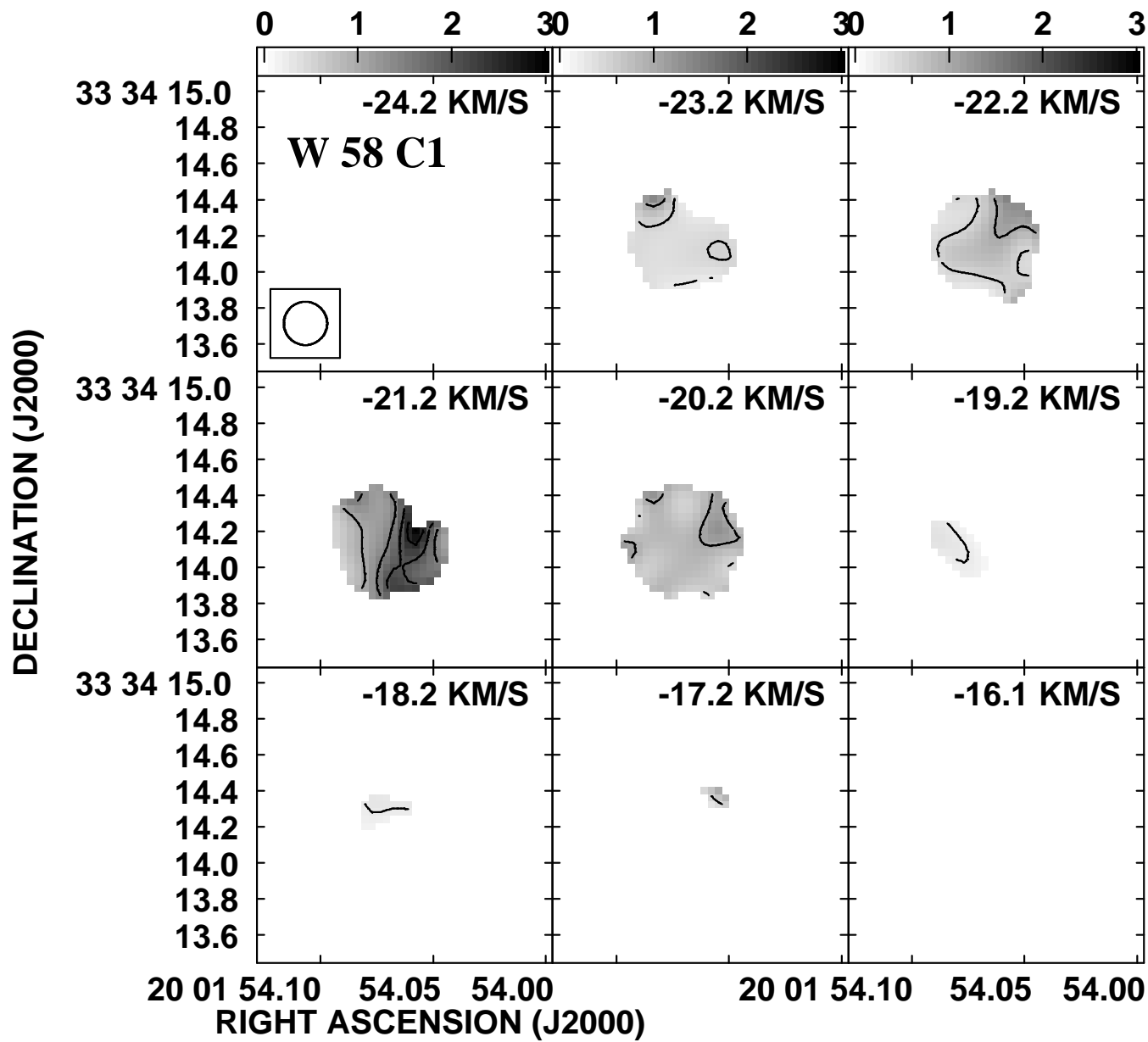
Parameter	Instrument	
	WSRT	VLA
Configuration	3 km	A array
H ₂ CO transition	1 ₁₀ – 1 ₁₁	2 ₁₁ – 2 ₁₂
Rest frequency(MHz)	4829.6596	14488.4788
Wavelength (cm)	6.21	2.07
Primary Beam (')	10.8	3.0
Source	W 58 (entire)	W 58 C
Field Center		
α (B1950)	19 ^h 59 ^m 54.00 ^s	19 ^h 59 ^m 58.48 ^s
δ (B1950)	33°24'30.0''	33°25'49.6''
α (J2000)	20 ^h 01 ^m 49.61 ^s	20 ^h 01 ^m 54.07 ^s
δ (J2000)	33°32'54.24''	33°34'14.17''
Dates of observations	1980 October 19	1985 January 18
Integration time (hr)	12	9
Number of telescopes	14	25
Number of channels	31	31
Velocities (LSR, km s ⁻¹)		
Central vel (ch 16)	-21.4	-21.2
Resolution	0.727	1.01
Channel spacing	0.606	1.01
Synthesized beam (")	7.2x3.8 (PA= 0.0°)	
Natural weight		0.253x0.224 (PA= -84.0°)
Uniform weight		0.106x0.098 (PA= -88.5°)

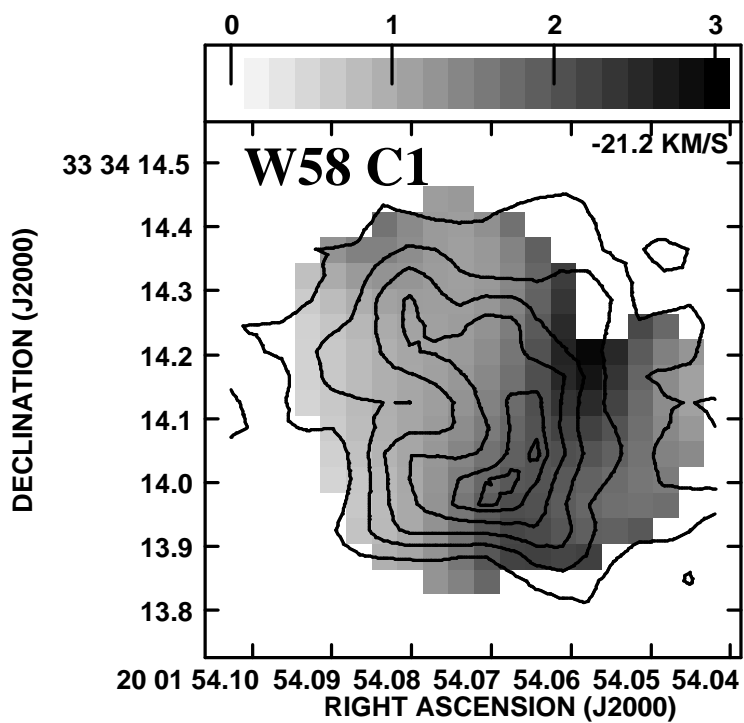




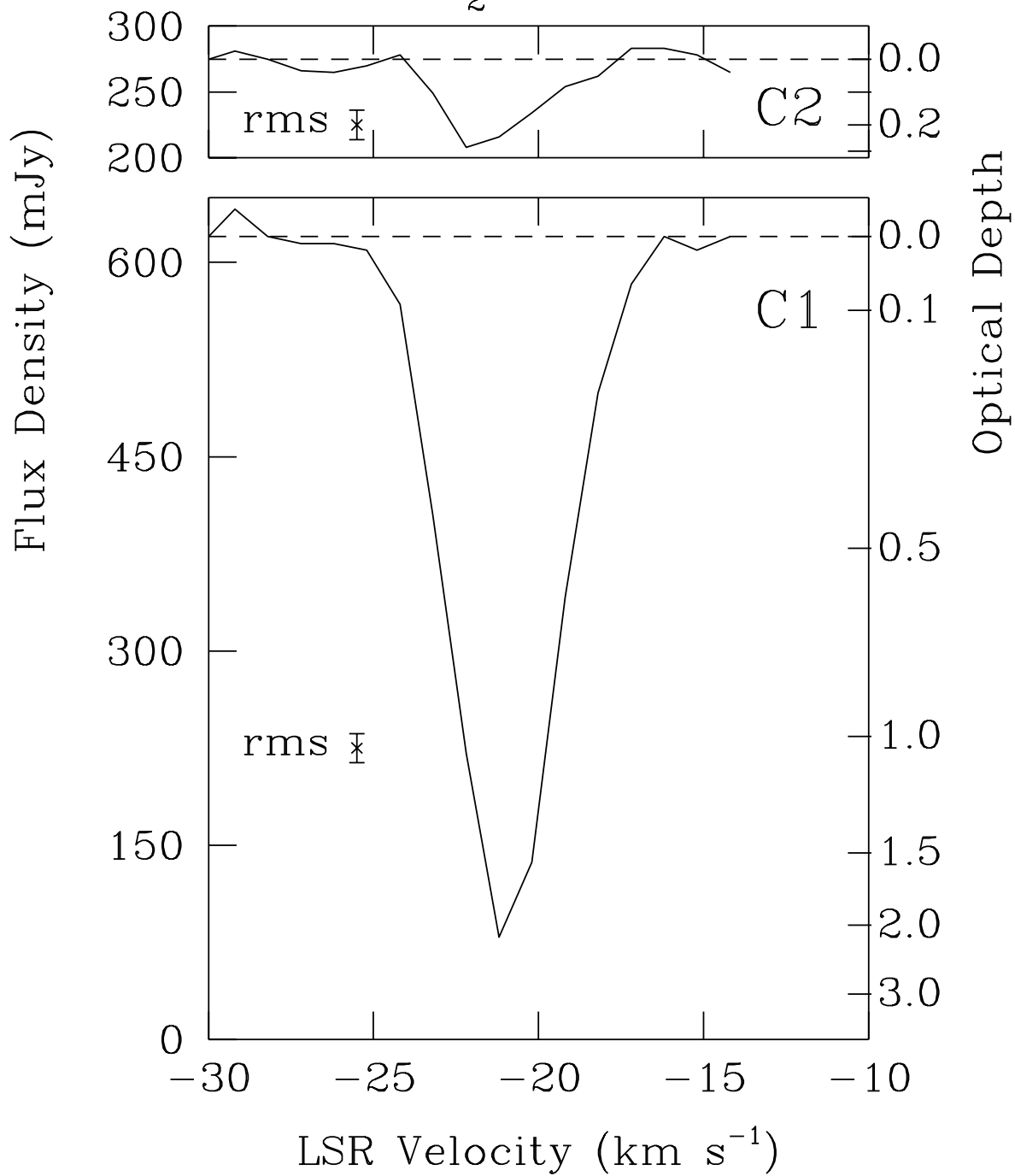








6 cm H₂CO W 58



2 cm H₂CO W 58

